Prussian Blue without Coordinated Water as Superior Cathode for Sodium-Ion Batteries

ARTICLE *in* CHEMICAL COMMUNICATIONS · MARCH 2015

Impact Factor: 6.83 · DOI: 10.1039/C5CC01180A

6 AUTHORS, INCLUDING:

Yu-Shi He
Shanghai Jiao Tong University
47 PUBLICATIONS **753** CITATIONS
SEE PROFILE

Zi-Feng Ma
Shanghai Jiao Tong University
163 PUBLICATIONS **2,373** CITATIONS
SEE PROFILE

ChemComm

COMMUNICATION

View Article Online
View Journal | View Issue

Cite this: *Chem. Commun.*, 2015, 51, 8181

Received 8th February 2015,
Accepted 26th March 2015

DOI: 10.1039/c5cc01180a

www.rsc.org/chemcomm

Prussian blue without coordinated water as a superior cathode for sodium-ion batteries†

Dezhi Yang,[a] Jing Xu,[a] Xiao-Zhen Liao,*[a] Hong Wang,[b] Yu-Shi He[a] and Zi-Feng Ma*[ab]

A micro-cubic Prussian blue (PB) without coordinated water is first developed by electron exchange between graphene oxide and PB. The obtained reduced graphene oxide–PB composite exhibited complete redox reactions of the Fe sites and delivered ultrahigh electrochemical performances as well as excellent cycling stability as a cathode in sodium-ion batteries.

Lithium-ion batteries (LIBs) have been proposed to be appropriate energy storage devices in electric vehicles (EVs) and large-scale energy storage systems (LESS).[1–3] However, the high cost and limited resources of lithium restrict their broader application. As a consequence of recent advances in cathode and anode materials, room-temperature rechargeable sodium-ion batteries (SIBs) have demonstrated great potential, especially in LESS. Compared with LIBs, SIBs are more sustainable because of the abundant sodium resources on Earth.[4–8] The development of electrode materials that are composed of simple, inexpensive and environmentally friendly elements and that exhibit high electrochemical performance would represent an important advancement of SIB technology.

Many pioneering studies have pointed to Prussian blue (PB) and its analogues (PBAs) as feasible cathode materials because of their open and zeolite-like framework, which allows Na^+ ions to pass through rapidly. Furthermore, PBAs exhibit high specific capacities and good cycling stabilities and can be prepared from eco-friendly raw materials *via* a simple synthetic process.[9–15] In the cubic framework of PB, the Fe site is bounded by $Fe(CN)_6$ groups. Thus, two types of Fe sites are present in the Fe–C≡N–Fe lattice framework: one with a C end in the low-spin state (Fe1) and another with an N end in the high-spin state (Fe2). The redox reactions of Fe1 and Fe2 should occur at different redox potentials with a similar number of coulombs consumed because the number of Fe1 sites is almost equal to the number of Fe2 sites. When PB is used as a cathode material in SIBs, two voltage plateaus with similar capacities corresponding to Fe1 and Fe2 should be observed. However, in most previous reports, the PB cathode only delivers one distinct voltage plateau at a potential less than 3.0 V, corresponding to Fe2; in contrast, the corresponding voltage plateau of Fe1 is inconspicuous or extremely short for reasons that remain unknown.[9,11,12] The redox potential of Fe1 is higher than that of Fe2. The insufficient reaction of Fe1 may result in decreased capacity and a low discharge medium voltage of SIBs. To promote the practical application of PB in SIBs, clarification of the aforementioned phenomenon is important to improve the PB's specific capacity and the charge/discharge voltage plateau of Fe1.

Herein, we first investigate the relationship between the coordinated water and the voltage plateau of Fe1 in PB. As far as we know, the literature contains no reports related to the negative effects of coordinated water on the electrochemical performance of PB, such as its discharge capacity and redox voltage during the insertion/extraction of Na^+. The main barrier is that the coordinated water located in the vacant sites of the framework is difficult to be removed by simple methods.[16] In this research, we developed an effective method to remove the coordinated water from the PB structure. Briefly, heat-treatment of a graphene oxide–PB composite (GOPC) released the coordinated water from the PB framework *via* electron exchange between the cubic PB particles and graphene oxide (GO) at high temperature.

The cubic, micron-sized PB was synthesised by self-decomposition of $Na_4Fe(CN)_6$ in hot, acidic solution (see S1 of ESI†). $Na_4Fe(CN)_6$ decomposed slowly to generate Fe^{2+}, which reacted with the $Fe(CN)_6$ group to form the well-shaped cubic PB, as shown in Fig. 1a. The chemical composition of the obtained PB was revealed to be $Na_{0.81}Fe[Fe(CN)_6]_{0.79}{*}\square_{0.21}$ ($\square$ = $Fe(CN)_6$ vacancy) by elemental analysis and inductively coupled plasma (ICP) analysis. The concentration of $Fe(CN)_6$ vacancies reached approximately 21% based on all $Fe(CN)_6$ sites in the perfect PB framework. In the hot acidic solution, $Fe(CN)_6^{4-}$ and Fe^{2+} can be oxidised to $Fe(CN)_6^{3-}$ and Fe^{3+}. Thus, the prepared PB product might contain some Fe^{3+}–$Fe(CN)_6^{4-}$, Fe^{3+}–$Fe(CN)_6^{3-}$ and Fe^{2+}–$Fe(CN)_6^{3-}$ bonds in addition to the main Fe^{2+}–$Fe(CN)_6^{4-}$ bonds

[a] *Shanghai Electrochemical Energy Devices Research Center, Department of Chemical Engineering, Shanghai Jiao Tong University, Shanghai, 200240, China. E-mail: zfma@sjtu.edu.cn, liaoxz@sjtu.edu.cn; Fax: +86 21 5474 1297; Tel: +86 21 5474 2894*

[b] *Sinopoly Battery Research Center, Shanghai, 200240, China*

† Electronic supplementary information (ESI) available. See DOI: 10.1039/c5cc01180a

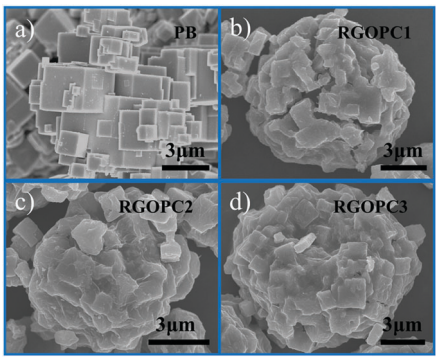

Fig. 1 Scanning electron microscopy images of (a) PB, (b) RGOPC1, (c) RGOPC2 and (d) RGOPC3.

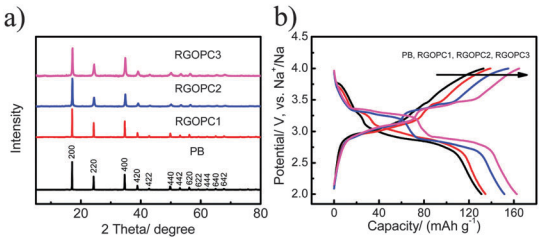

Fig. 2 (a) X-ray diffraction patterns of PB, RGOPC1, RGOPC2 and RGOPC3. (b) The second galvanostatic charge–discharge profiles of PB, RGOPC1, RGOPC2 and RGOPC3 between 2.0 V and 4.0 V at 30 mA g^{-1}.

in the crystal framework. Thermogravimetric analysis (TG) showed that the water content of the PB was 11.5 wt% (see S2 of ESI†). Absorbed water, zeolitic water and coordinated water were all present in the PB. The zeolitic water was just physically adsorbed in the interstitial lattice sites. However, the coordinated water bound to the Fe ions might affect the surrounding electronic states of the Fe ions or the $Fe(CN)_6$ groups.

To ensure that the PB particles were in good contact with the GO flakes, graphene oxide–PB composites (GOPCs) with different GO contents (the GOPC with 9 wt% GO as GOPC3, the GOPC with 5.7 wt% GO as GOPC2 and the GOPC with 2.9 wt% GO as GOPC1) were fabricated using a spray-drying method. The GOPCs were then heat treated at 220 °C to form reduced graphene oxide (RGO)–PB composites (RGOPCs) with a lower concentration of coordinated water.[17] Fig. 1b–d show SEM images of the prepared RGOPCs with different RGO contents. On the basis of the chemical composition of $Na_{0.81}Fe[Fe(CN)_6]_{0.79}{*}\square_{0.21}$, 1.79 Fe ions correspond to six C ions. Hence, the remainder of the carbon in the RGOPCs detected by elemental analysis belongs to RGO. The specific RGO contents of the RGOPCs were analysed to be 6.2 wt% (RGOPC3) for a 9 wt% original GO content, 3.9 wt% (RGOPC2) for a 5.7 wt% original GO content, and 1.4 wt% (RGOPC1) for a 2.9 wt% original GO content, respectively. The PB was clearly well covered when the RGO content was 6.2 wt% RGO, but was only partly covered when the RGO content was 1.4 wt%. The size of the secondary particles reached approximately 7–10 μm, which is suitable for industrial applications. Compared with GOPC3, RGOPC3 manifested inconspicuous changes in its SEM images (see S3 of ESI†). Fig. 2a shows the X-ray diffraction (XRD) patterns of the PB and the RGOPCs. The patterns of these samples exhibit a well-defined face-centred cubic (fcc) structure (space group $Fm\bar{3}m$) with sharp and strong diffraction peaks.[11]

Interestingly, the electrochemical performances of pure PB and RGOPCs were remarkably different, as shown in the charge–discharge curves of pure PB and the RGOPCs (Fig. 2b). The pure PB only delivered one voltage plateau at 2.73 V, with a specific discharge capacity of 131.2 mA h g^{-1} (30 mA g^{-1}). The curves of RGOPC2 and RGOPC3 exhibited two distinct voltage plateaus at 2.73 V and 3.2–3.4 V and specific discharge capacities of 152 mA h g^{-1} and 163.3 mA h g^{-1} at 30 mA g^{-1}, respectively. The voltage plateau of 3.2–3.4 V corresponded to the redox of Fe1, whereas that at 2.7–3 V corresponded to Fe2. However, RGOPC1 exhibited only a small voltage plateau for Fe1, with a specific discharge capacity of 135 mA h g^{-1} (30 mA g^{-1}). According to the following redox reaction in SIBs,

$$Fe[Fe(CN)_6]_{0.79} + 1.79Na \leftrightarrow Na_{1.79}Fe[Fe(CN)_6]_{0.79} - 1.79e^-$$

the theoretical capacity of PB with a complete redox reaction was calculated to be 181.3 mA h g^{-1}. The low discharge capacity of pure PB may be a consequence of only a portion of the Fe1 sites corresponding to the insertion/exaction of Na^+. However, in RGOPC2 and RGOPC3, the Fe1 sites can react fully. These are confirmed by the Mössbauer spectra of charged PB and charged RGOPC3, as shown in Fig. S4 (ESI†). Obviously, the $Fe1^{3+}$ sites in the charged RGOPC3 are more than the charged PB. There are still some $Fe1^{2+}$ sites in the charged PB structure.[18,19] Consistent with the beneficial role of RGO,[7,20] the high discharge capacity of RGOPC3 is close to the theoretical capacity of PB and can thus be considered a very promising cathode material for SIBs.

The cyclic voltammograms of PB and RGOPC3 in the range of 2–4 V *vs.* Na/Na^+ at a scan rate of 0.3 mV s^{-1} (Fig. S3a, ESI†) are consistent with their charge/discharge performances. The voltammogram of PB exhibits a single, large redox peak at 2.67 V/3.06 V and a series of small redox peaks at higher potentials. The voltammogram of RGOPB3 shows three main redox peaks; the peaks at 2.75 V/3.17 V correspond to the oxidation–reduction of the Fe2 sites, whereas the two adjacent redox peaks at 3.17 V/3.43 V and 3.26 V/3.52 V correspond to the redox processes of the Fe1 sites. The small peak separation may due to the differences in the surrounding crystal structure of the Fe1 site with or without vacancy defects.[21]

The greatly improved electrochemical performances of RGOPCs compared to the performance of pure PB may due to the decrease in the amount of coordinated water in the PB of RGOPCs. This hypothesis was validated by the Fourier-transform infrared (FT-IR) spectra of the coordinated water in the RGOPCs and PB samples, as shown in Fig. S3b (ESI†). The small peaks at 3556 cm^{-1}, 3594 cm^{-1} and 3627 cm^{-1} are assigned to the coordinated water in the PB framework.[22–24] The peaks of the coordinated water in the spectrum of RGOPC3 became weak and almost disappeared compared to those in the spectrum of pure PB; *i.e.*, the amount of coordinated water in the RGOPCs was decreased to some extent during the co-heating of GO and PB. The RGOPCs might still contain coordinated water, but it could not be measured precisely. Nonetheless, on the basis of the charge–discharge curves of RGOPCs, we concluded that the

residual water in the PB framework only slightly affected the electrochemical performance of RGOPC2 and RGOPC3 in SIBs.

The removal of coordinated water was further confirmed by the Rietveld refinement results of the XRD patterns. These XRD patterns of PB and RGOPCs were refined using GSASΠ software, as shown in Fig. S5 and Table S1 (ESI†).[25–27] The fitted XRD patterns indicate that all samples are in the single crystalline phase. In the fcc structure of the samples, the Fe2 site is located at the **4a** (0, 0, 0) crystallographic position, while the Fe1 site occupies the **4b** (1/2, 1/2, 1/2) crystallographic position. From Table S1 (ESI†), the amount of O atoms in RGOPC3 decreased when compared with PB, indicating that the coordinated water was removed in RGOPC3 and the amount of vacancies increased from PB to RGOPC3. The *d*-spacings of these samples are 10.3423 Å for PB, 10.3361 Å for RGOPC1, 10.2735 Å for RGOPC2 and 10.2591 Å for RGOPC3, respectively, which are big enough for Na^+ to pass through. The decreased lattice parameter for RGOPC3 may be due to the fact that the removal of water generates the cation vacancies and then affects the residual stress of the crystals.

A possible mechanism for removing coordinated water from PB is shown in Fig. 3 (see S7 and S8 of ESI†). At a high temperature (220 °C), Fe1 and Fe2 in the PB structure are active and easily lose or gain electrons, especially in the case of Fe2 because of the low bond strength of Fe–N≡C.[28] The oxide group acquires one electron from $Fe2^{2+}$ in the external PB crystal to break from the GO first, and $Fe2^{2+}$ is oxidised to $Fe2^{3+}$. Then, the PB requires an additional electron or cation vacancy to maintain electrical neutrality. The PB framework contains numerous $Fe(CN)_6$ vacancies substituted by $(H_2O)_6$ clusters.[28,29] These clusters are referred to as $[Fe2^{2+}(NC)_5(OH_2)]_6$, which hinders the insertion/extraction of Na^+. The Fe2 site of $Fe2^{2+}(NC)_5(OH_2)$, which is surrounded by nitrogen and oxygen atoms, experiences a weak ligand field and probably provides favourable electronic energy levels that can compensate the electric change by removing the (OH_2) sites to form cation vacancies.[16,28,30–32] Consequently, the coordinated water can be eliminated by the heat treatment of the GOPCs. The charge–discharge curves in Fig. 2b indicate that the original 2.9 wt% GO content cannot completely eliminate the negative effects of the coordinated water, whereas the original 5.7 wt% GO content in the RGOPC is sufficient to provide good electrochemical performance.

In order to analyse the changes in the Fe1 site and the Fe2 site, we measured the Mössbauer spectra of pristine PB and RGOPC3 (Fig. 4a and b). The fitted curves are also presented. Table S2 (ESI†) summarizes the fitted parameters. From Fig. 4a and b, $Fe1^{2+}/Fe1^{3+}$ in PB and RGOPC3 is calculated to be 4.64 and 2.23, while $Fe2^{2+}/Fe2^{3+}$ is calculated to be 2.95 and 1.33, respectively.[18,19]

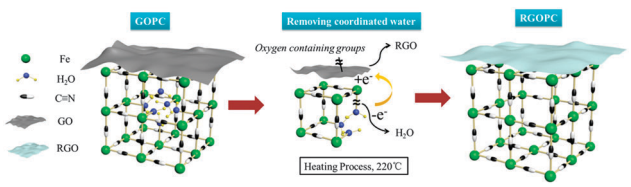

Fig. 3 A schematic mechanism for the removal of coordinated water from RGOPC.

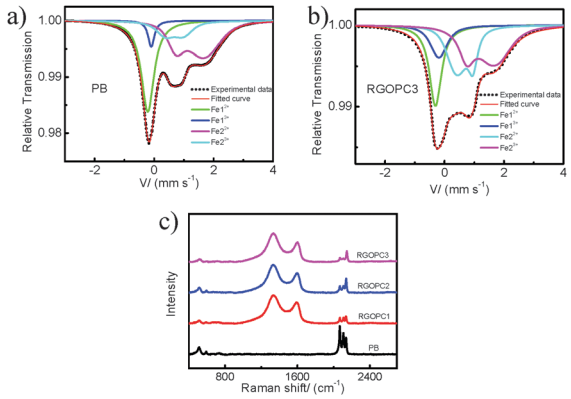

Fig. 4 (a) Mössbauer spectrum of PB. (b) Mössbauer spectrum of RGOPC3. (c) Raman spectra of PB, RGOPC1, RGOPC2 and RGOPC3.

The increased amounts of $Fe1^{3+}$ and $Fe2^{3+}$ in RGOPC3 are consistent with the mechanism for the removal of coordinated water. The Raman spectra present similar results, as shown in Fig. 4c. The $Fe(CN)_6^{4-}/Fe(CN)_6^{3-}$ ratios were calculated to be 3.29, 2.51, 1.35 and 1.14 for PB, RGOPC1, RGOPC2 and RGOPC3, respectively (see S10 and S11 of ESI†). The number of $Fe(CN)_6^{3-}$ groups in the PB framework increased because of charge transfer between the Fe1 site and the Fe2 site through the C≡N bridge.[30] In the adjacent sites of the formed cation vacancies, the cation vacancies functioned as electron-withdrawing sites to induce the redox reactions of $Fe1^{2+}$–C≡N–$Fe2^{3+}$ and $Fe1^{3+}$–C≡N–$Fe2^{2+}$, thereby decreasing the $Fe(CN)_6^{4-}/Fe(CN)_6^{3-}$ ratio. Therefore, these reactions can occur from the surface to the interior of the PB particles, as confirmed by the Raman spectra of RGOPC3 heated for different times (see S12 of ESI†). The ratio of $Fe(CN)_6^{4-}/Fe(CN)_6^{3-}$ in RGOPC3 decreased as the heating time was increased.

The electrochemical performances of RGOPCs were investigated further. Fig. 5a compares the long-term cycling performances of RGOPCs with pure PB at a current density of 200 mA g^{-1} and in the potential range between 2.0 and 4.0 V. The RGOPCs clearly exhibited remarkably improved cycling performance. The initial discharge capacities of RGOPC3, RGOPC2 and RGOPC1 were 149.7 mA h g^{-1}, 130 mA h g^{-1} and 110.9 mA h g^{-1}, with capacity retentions of 91.9% (137.6 mA h g^{-1}), 88.8% (115.5 mA h g^{-1}) and 71.6% (79.43 mA h g^{-1}), respectively, after 500 cycles. The pure PB only delivered an initial discharge capacity of 101.6 mA h g^{-1}, with a capacity retention of 57.5% (58.4 mA h g^{-1}) after 500 cycles.

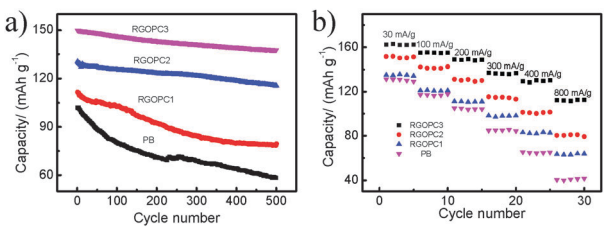

Fig. 5 (a) Cycling performances of PB, RGOPC1, RGOPC2 and RGOPC3 between 2.0 V and 4.0 V at 200 mA g^{-1}. (b) The rate performance of PB, RGOPC1, RGOPC2 and RGOPC3 at different current densities between 2 V and 4 V.

Notably, the RGOPC3 sample exhibited the most attractive performance among all of the investigated samples. Furthermore, when RGOPC3 was placed in water again and then dried under vacuum, its charge–discharge curve still exhibited two obvious voltage plateaus for Fe1 and Fe2 (see S13 of ESI†). This phenomenon indicates that the framework of RGOPC3 was stable and in good order after the coordinated water was removed; the vacancies were not refilled by water.

In addition to the water removal effect, the superior electrical conductivity of RGO also greatly contributed to the rate performance of the RGOPCs. Fig. 5b shows the discharge capacities of the RGOPC and pure PB samples charged/discharged at different current densities between 2.0 and 4.0 V *vs.* Na^+/Na. The RGOPC3 electrode clearly exhibited the best rate performance, especially at high current densities. The average discharge capacity of the RGOPC3 cathode was 112 mA h g^{-1} at a current density of 800 mA g^{-1}. In contrast, the discharge capacity of the pure PB electrode was only 41 mA h g^{-1} under the same discharge conditions. Fig. S13b (ESI†) shows the electrochemical impedance spectra of PB and RGOPCs after ten charge–discharge cycles at 200 mA g^{-1}. RGOPC3 exhibited the lowest charge transfer resistance, consistent with its rate performance.

In summary, we successfully synthesised RGOPCs with coordinated water removed by thermal heating of GO–PB composites. We first demonstrated the relationship between the coordinated water and the redox voltage plateau of Fe1, which is significant for SIBs. During the co-heating process of GO and PB, the oxide group of GO acquired one electron from the Fe2 site of $Fe2^{2+}(NC)_5(OH_2)$ in PB to deviate from GO. Then, the (OH_2) of $Fe2^{2+}$–$(NC)_5(OH_2)$, which experienced a weak ligand field, was removed to form a cation vacancy to compensate the electric change of $Fe2^{2+/3+}$ in the PB framework. Meanwhile, the cation vacancies functioned as electron-withdrawing sites to induce redox reactions of $Fe1^{2+}$–C≡N–$Fe2^{3+}$ and $Fe1^{3+}$–C≡N–$Fe2^{2+}$ through the C≡N bridge. Accompanied by this process, the coordinated water in the $Fe(CN)_6$ vacancies was removed. When RGOPC3 was used as a cathode in SIBs, it delivered a high specific capacity of 163.3 mA h g^{-1} (30 mA g^{-1}), which is close to the theoretical specific capacity of PB, with two voltage plateaus for Fe1 and Fe2; in contrast, the pure PB exhibited a specific capacity of only 131.2 mA h g^{-1} (30 mA g^{-1}), with one obvious voltage plateau for Fe2. Thus, almost all of the redox sites in RGOPC3 corresponded to the insertion/exaction of Na^+, whereas only portion of the redox sites in PB corresponded to the Na^+ insertion/exaction. RGOPC3 also exhibited excellent cycling stability and good rate properties, with a specific capacity of 112 mA h g^{-1} at a current density of 800 mA g^{-1}. After 500 cycles, the capacity retention of the RGOPC3 cathode still reached 91.9% at 200 mA h g^{-1}. Hence, the high rate performance and excellent cycling stability strongly suggest that RGOPC3 is a feasible cathode material for SIBs. Furthermore, the relationship between the coordinated water and low-spin Fe sites of $Fe(CN)_6$ is also significant for other similar materials, especially PBAs when they are used in SIBs.

The authors appreciate the financial support from the Natural Science Foundation of China (21336003 and 21073120), the Major Basic Research Program of China (2014CB239700), the Science and Technology Commission of Shanghai Municipality (14DZ2250800), and the Shanghai Natural Science Foundation (15ZR1422300).

Notes and references

1 B. Dunn, H. Kamath and J. M. Tarascon, *Science*, 2011, **334**, 928.
2 Z. G. Yang, J. L. Zhang, M. C. W. Kintner-Meyer, X. C. Lu, D. W. Choi, J. P. Lemmon and J. Liu, *Chem. Rev.*, 2011, **111**, 3577.
3 J. B. Goodenough and Y. Kim, *Chem. Mater.*, 2010, **22**, 587.
4 J. Liu, J. G. Zhang, Z. G. Yang, J. P. Lemmon, C. Imhoff, G. L. Graff, L. Y. Li, J. Z. Hu, C. M. Wang, J. Xiao, G. Xia, V. V. Viswanathan, S. Baskaran, V. Sprenkle, X. L. Li, Y. Y. Shao and B. Schwenzer, *Adv. Funct. Mater.*, 2013, **23**, 929.
5 H. Pan, Y.-S. Hu and L. Chen, *Energy Environ. Sci.*, 2013, **6**, 2338.
6 V. Palomaresa, P. Serras, I. Villaluenga, K. B. Hueso, J. Carretero-González and T. Rojo, *Energy Environ. Sci.*, 2012, **5**, 5884.
7 D. Yang, J. Xu, X.-Z. Liao, Y.-S. He, H. Liu and Z.-F. Ma, *Chem. Commun.*, 2014, **50**, 13377.
8 K. B. Hueso, M. Armand and T. Rojo, *Energy Environ. Sci.*, 2013, **6**, 734.
9 Y. Lu, L. Wang, J. Cheng and J. B. Goodenough, *Chem. Commun.*, 2012, **48**, 6544.
10 C. D. Wessells, R. A. Huggins and Y. Cui, *Nat. Commun.*, 2011, **2**, 550.
11 Y. You, X.-L. Wu, Y.-X. Yin and Y.-G. Guo, *Energy Environ. Sci.*, 2014, **7**, 1643.
12 X. Wu, W. Deng, J. Qian, Y. Cao, X. Ai and H. Yang, *J. Mater. Chem. A*, 2013, **1**, 10130.
13 Y. Yue, A. J. Binder, B. Guo, Z. Zhang, Z.-A. Qiao, C. Tian and S. Dai, *Angew. Chem., Int. Ed.*, 2014, **53**, 3134.
14 M. Okubo, C. H. Li and D. R. Talham, *Chem. Commun.*, 2014, **50**, 1353.
15 L. Zhang, L. Chen, X. Zhou and Z. Liu, *Adv. Energy Mater.*, DOI: 10.1002/aenm.201400930.
16 A. Kumar and S. M. Yusuf, *Phys. Rev. B: Condens. Matter Mater. Phys.*, 2005, **71**, 054414.
17 G.-W. Zhou, J. Wang, P. Gao, X. Yang, Y.-S. He, X.-Z. Liao, J. Yang and Z.-F. Ma, *Ind. Eng. Chem. Res.*, 2013, **52**, 1197.
18 K. Itaya, T. Ataka, A. Toshima and T. Shlnohara, *J. Phys. Chem.*, 1982, **86**, 2415.
19 E. Reguera, J. Fernández-Bertrán, A. Dago and C. Diaz, *Hyperfine Interact.*, 1992, **73**, 295.
20 X. Zhu, Y. Zhu, S. Murali, M. D. Stoller and R. S. Ruoff, *ACS Nano*, 2011, **5**, 3333.
21 H. Ishiyama, G. Maruta, T. Kobayashi and S. Takeda, *Polyhedron*, 2003, **22**, 1981.
22 M. Miyazaki, A. Fujii, T. Ebata and N. Mikami, *Science*, 2004, **304**, 1134.
23 J.-W. Shin, N. I. Hammer, E. G. Diken, M. A. Johnson, R. S. Walters, T. D. Jaeger, M. A. Duncan, R. A. Christie and K. D. Jordan, *Science*, 2004, **304**, 1137.
24 M. Liu, X. F. Bian, Y. F. Xia, Z. Bao, H. S. Wu and M. X. Xu, *Curr. Appl. Phys.*, 2011, **11**, 271.
25 J. C. Pramudita, S. Schmid, T. Godfrey, T. Whittle, M. Alam, T. Hanley, H. E. A. Brand and N. Sharma, *Phys. Chem. Chem. Phys.*, 2014, **16**, 24178.
26 P. Bhatt, N. Thakur, M. D. Mukadam, S. S. Meena and S. M. Yusuf, *J. Phys. Chem. C*, 2013, **117**, 2676.
27 B. H. Toby, *J. Appl. Crystallogr.*, 2001, **34**, 210.
28 P. R. Bueno, D. Giménez-Romero, F. F. Ferreira, G. O. Setti, J. J. García-Jareño, J. Agrisuelas and F. Vicente, *J. Phys. Chem. C*, 2009, **113**, 9916.
29 P. R. Bueno, D. Giménez-Romero, C. Gabrielli, J. J. García-Jareño, H. Perrot and F. Vicente, *J. Am. Chem. Soc.*, 2006, **128**, 17146.
30 L. Samain, B. Gilbert, F. Grandjean, G. J. Long and D. Strivay, *J. Anal. At. Spectrom.*, 2013, **28**, 524.
31 J. C. Pramudita, S. Schmid, T. Godfrey, T. Whittle, M. Alam, T. Hanley, H. E. A. Brand and N. Sharma, *Phys. Chem. Chem. Phys.*, 2014, **16**, 24178.
32 F. Herren, P. Fischer, A. Ludi and W. Hälg, *Inorg. Chem.*, 1980, **19**, 956.

